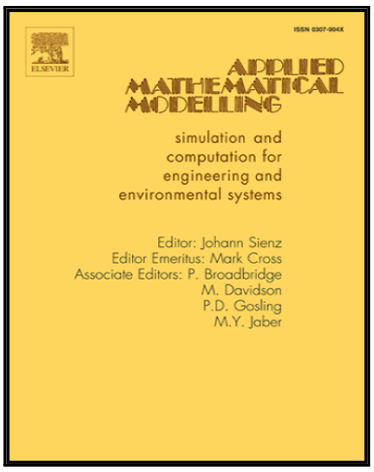

Discretization of the divergence formulation of the bed slope term in the shallow-water equations and consequences in terms of energy balance

Martin Bruwier , Pierre Archambeau , Sébastien Erpicum , Michel Pirotton , Benjamin Dewals

PII: S0307-904X(16)30037-3
DOI: 10.1016/j.apm.2016.01.041
Reference: APM 11001

To appear in: *Applied Mathematical Modelling*

Received date: 15 April 2015
Revised date: 13 January 2016
Accepted date: 20 January 2016

Please cite this article as: Martin Bruwier , Pierre Archambeau , Sébastien Erpicum , Michel Pirotton , Benjamin Dewals , Discretization of the divergence formulation of the bed slope term in the shallow-water equations and consequences in terms of energy balance, *Applied Mathematical Modelling* (2016), doi: 10.1016/j.apm.2016.01.041

Highlights

- We quantify energy variations for multiple discretizations of the bed slope term.
- Our analysis covers a wide range of ambient Froude numbers and topographic steps.
- We propose an optimal discretization minimizing the energy variation.
- The optimal discretization is shown valid for a wide range of flows and topography.
- Two numerical tests show results in agreement with our theoretical analysis.

Discretization of the divergence formulation of the bed slope term in the shallow-water equations and consequences in terms of energy balance

Martin Bruwier, PhD Student, *Hydraulic in Environmental and Civil Engineering (HECE), University of Liege (ULG), Liege, Belgium*

Email: mbruwier@ulg.ac.be (author for correspondence)

Pierre Archambeau, Research Associate, *Hydraulic in Environmental and Civil Engineering (HECE), University of Liege (ULG), Liege, Belgium*

Email: Pierre.Archambeau@ulg.ac.be

Sébastien Erpicum, Assistant Professor, *Hydraulic in Environmental and Civil Engineering (HECE), University of Liege (ULG), Liege, Belgium*

Email: S.Erpicum@ulg.ac.be

Michel Pirotton, Full Professor, *Hydraulic in Environmental and Civil Engineering (HECE), University of Liege (ULG), Liege, Belgium*

Email: Michel.Pirotton@ulg.ac.be

Benjamin Dewals, Assistant Professor, *Hydraulic in Environmental and Civil Engineering (HECE), University of Liege (ULG), Liege, Belgium*

Email: B.Dewals@ulg.ac.be

Running Head: Discretization of the divergence formulation of the bed slope term

Discretization of the divergence formulation of the bed slope term in the shallow-water equations and consequences in terms of energy balance

ABSTRACT

In this research, the influence on energy balance of the discretization scheme of the divergence formulation of the bed slope term in the shallow-water equations is analysed theoretically (for a single topographic step) and based on two numerical tests. Different values of the main parameter controlling the discretization scheme of the divergence formulation are analysed to identify the formulation which minimizes the energy variation resulting from the discretization. For a wide range of ambient Froude numbers and relative step heights, the theoretical value of the control parameter minimizing the energy variation falls within a very narrow range, which can reasonably be approximated by a single "optimal" value. This is a result of high practical relevance for the design of accurate numerical schemes, as confirmed by the results of the numerical tests.

Keywords: bed slope term; divergence formulation; discretization schemes; energy balance; flux-vector splitting; shallow-water.

1 Introduction and background

The shallow-water equations (SWE) constitute the state-of-the-art for large-scale modelling of a wide range of flow in hydraulic engineering and fluvial hydraulics [5,7,8,26,27,35], as well as for applications in other fields such as coastal engineering [30] or geophysical flow [29].

For a prismatic channel with a rectangular cross-section without lateral inflow nor outflow, the one dimensional (1D) SWE write:

$$\begin{cases} \dfrac{\partial h}{\partial t}+\dfrac{\partial q}{\partial x}=0 \\ \dfrac{\partial q}{\partial t}+\dfrac{\partial}{\partial x}\left(\dfrac{q^2}{h}+g\dfrac{h^2}{2}\right)=S_i-S_f \end{cases} \tag{1}$$

with g the gravitational acceleration, h the water depth, q the specific discharge, t the time, x the spatial coordinate, S_i the bed slope source term and S_f the friction term.

In Eq. (1), the advective terms and the pressure gradient are written in divergence form, which is perfectly suitable for the application of a conservative numerical discretization, such as the finite volume method. In contrast, the bed slope source term S_i writes in a non-conservative form:

$$S_i=-gh\partial z_b/\partial x \tag{2}$$

with z_b the bottom elevation. This formulation is referred hereafter as the standard

formulation of the bed slope source term (SFB).

For general hyperbolic conservation laws with source terms, Bermúdez and Vázquez [4] introduced the concept of upwind discretization of the source terms. The goal is to make the discretization of the source terms consistent with the discretization of the advective and pressure terms, so as to obtain a so-called well-balanced scheme. In the discretization of the SWE, this approach enables the preservation of an initial solution corresponding to quiescent water over an irregular bottom [24]. The results obtained with well-balanced schemes were shown to be more accurate than those obtained with a simple pointwise evaluation [14]. This method has been extended for unstructured meshes [3], quasi-steady problems [20], flux-difference splitting schemes [14,17,34] and flux-vector splitting schemes [21,13,31]. A comparative analysis of different topography discretization techniques has been performed by Kesserwani [18].

From the work of Zhou et al. [36] on the surface gradient method, in which variables reconstruction is based on the free surface level instead of the water depth, Valiani and Begnudelli [32] introduced a divergence formulation of the bed slope term (DFB). It consists in evaluating the bed slope term as the spatial variation of the pressure assuming a uniform water level η_0 :

$$S_i = \frac{\partial}{\partial x}\left(\frac{1}{2}gh^2\right)_{\eta_0} \tag{3}$$

where η is the free surface level. f_{η_0} means that f is evaluated for a stationary water level $\eta = \eta_0$.

This treatment of the bed slope term similarly to a flux term (instead of a source term) is particularly useful in domains with a highly discontinuous topography, such as in urban areas [19,25,26].

While Eq. (1) is close to a conservative formulation, the assumption of a locally uniform water level η_0 in each cell induces discontinuities between two adjacent cells if the water level η is actually inclined.

Whereas Eq. (3) has been derived independently from any numerical scheme and kind of discretization, the discretization of the DFB was shown very convenient when using a structured grid with quadrilateral cells [32,33]. Recently, Hou et al. [15,16] extended the discretization of the DFB to unstructured grids.

The well-balanced discretization of the bed slope source term, as introduced by Nujic [24] and others, enables water at rest to be properly reproduced; but still numerical errors occur in the energy balance. Indeed, although the mathematical expressions of momentum

and energy conservation are equivalent for isothermal and incompressible flow, their discretized formulations do not lead to the same numerical results. The specific formulation used for the discretization of the bed slope term in the momentum equations has a substantial influence on the numerical errors induced in the energy balance. In the context of Godunov-type solvers, Murillo and Garcia Navarro [22] introduced a specific formulation of the bed slope source term ensuring energy conservation by using a linear combination of the integral and differential formulations of this term. The parameter controlling the linear combination depends on the variations of the flow variables and on the flow regime. Under steady conditions, the resulting scheme verifies the energy conservation for continuous and frictionless flow conditions, and the momentum balance in case of hydraulic jumps. Murillo and Garcia Navarro [23] generalized this method for flow in 1D non-prismatic channels of arbitrary cross-section. However, the approach developed by Murillo and Garcia Navarro [22,23] is not straightforward to extend to the DFB, as the resulting expression for η_0 may lead to singularities, as shown in supplementary material.

So far, in all studies based on the DFB, at the knowledge of the authors, the uniform water level η_0 within a cell was evaluated as the average flow depth plus the average bed elevation of the cell [32] or as the average of the free surface levels at the edges of this cell [15,33]. In contrast, in the present research, we evaluate the uniform water level η_0 as a linear combination of the free surface levels at the edges of the cell, taking into account specific features of the flux-vector splitting technique considered here. Different values of the parameter involved in the linear combination are analysed and benefit is taken from this extra degree of freedom to identify the value of this parameter which leads to the minimum error in the energy balance. First, a theoretical analysis is performed for a 1D slopeless and frictionless channel with a topographic step (similarly to the work of Stelling and Duinmeijer [28]). Second, the sensitivity of the numerical results to the value of the control parameter is analysed for a 1D steady flow over a bump and for a 1D dam break flow in a channel with a bump, with and without friction. A remarkable agreement is obtained between the conclusions of the theoretical analysis and the results of the numerical test cases.

2 Theoretical analysis

With the DFB, the momentum equation (Eq. 1) for a 1D steady solution without friction writes:

$$\frac{\partial}{\partial x}\left(\frac{q^2}{h}\right)+\frac{g}{2}\frac{\partial h^2}{\partial x}=\frac{g}{2}\frac{\partial h_{\eta_0}^2}{\partial x} \tag{4}$$

and the conservation of mechanical energy gives:

$$\frac{1}{2}\frac{\partial}{\partial x}\left(\frac{q^2}{h^2}\right)+g\frac{\partial h}{\partial x}=-g\frac{\partial z_b}{\partial x}. \quad (5)$$

We propose here a simpler approach in which the constant free surface elevation $\eta_{0,i}$ within cell i is computed as a linear combination of the free surface levels η_i and η_{i+1} with a constant parameter α:

$$\eta_{0,i}=(1-\alpha)\eta_i+\alpha\eta_{i+1} \quad (6)$$

The influence of the discretization of the bed slope term on the energy conservation is analysed in the case of steady flow in a 1D slopeless and frictionless channel with a topographic step (Fig. 1), as considered by Erpicum [10]. The water depths upstream and downstream of the bottom step are respectively called h_U and h_D. The topographic variation is referred to as Δz_b. On both sides of the topographic step, the specific discharge q is assumed constant and uniform.

2.1 Methods

Reference solution

For a flow without energy dissipation (neither friction nor hydraulic jump), the conservation of the mechanical energy (Eq. 5) between the upstream side E_U and the downstream side E_D of the topographic step writes [6,13]:

$$E_U=\frac{q^2}{2gh_U^2}+h_U=\frac{q^2}{2gh_D^2}+h_D+\Delta z_b=E_D \quad (7)$$

Using the following non-dimensional parameters:

$$\mathsf{F}_U^2=\frac{q^2}{gh_U^3},\quad \mathsf{h}=\frac{h_D}{h_U},\quad \Delta\mathsf{z}_b=\frac{\Delta z_b}{h_U},\quad \mathsf{F}_D^2=\frac{q^2}{gh_D^3}=\frac{\mathsf{F}_U^2}{\mathsf{h}^3} \quad (8)$$

Eq. (7) writes:

$$\mathsf{h}^3-\mathsf{h}^2\left(\frac{\mathsf{F}_U^2}{2}+1-\Delta\mathsf{z}_b\right)+\frac{\mathsf{F}_U^2}{2}=0 \quad (9)$$

This third order polynomial in h has two positive roots and one negative. Because Eq. (9) is valid for flows without hydraulic jump, only the root which preserves the same flow regime on either sides of the topographic step is considered here.

Discrete formulation of the DFB term

Consistently with the upwinding of the pressure terms towards downstream, the discretization of the DFB in cell i writes:

$$\frac{g}{2}\left[\frac{\partial h_{\eta_0}^2}{\partial x}\right]_{discr.,i} = \frac{g}{2}\frac{\left[(1-\alpha)\eta_i + \alpha\eta_{i+1} - z_{b,i+1}\right]^2 - \left[(1-\alpha)\eta_i + \alpha\eta_{i+1} - z_{b,i}\right]^2}{\Delta x} = -g\frac{\left[2\left[(1-\alpha)h_i + \alpha h_{i+1}\right] + (1-2\alpha)\left(z_{b,i} - z_{b,i+1}\right)\right]}{2}\frac{z_{b,i+1} - z_{b,i}}{\Delta x}. \quad (10)$$

This generalized discretization of the DFB contains two important particular cases.

Let's look at the following two particular cases, namely $\alpha = 0$ and $\alpha = 1/2$:

If $\alpha = 0$, Eq. (10) becomes:

$$\frac{g}{2}\left[\frac{\partial h_{\eta_0}^2}{\partial x}\right]_{discr.,i} = -g\frac{2h_i + z_{b,i} - z_{b,i+1}}{2}\frac{z_{b,i+1} - z_{b,i}}{\Delta x}. \quad (11)$$

This particular discretization is referred hereafter as the standard discretization of the DFB, as used by Valiani and Begnudelli [32] and presented by these authors as very simple and requiring low computational effort. In contrast, if $\alpha = 1/2$, Eq. (10) reduces to:

$$\frac{g}{2}\left[\frac{\partial h_{\eta_0}^2}{\partial x}\right]_{discr.,i} = -g\frac{h_i + h_{i+1}}{2}\frac{z_{b,i+1} - z_{b,i}}{\Delta x}. \quad (12)$$

This result is equivalent to the discretization of the SFB by Nujic [24] and Erpicum et al. [12]. This discretization is analogous to the ones used by Valiani and Begnudelli [33] and by Hou et al. [15]. Hereafter, this discretization is referred to as the standard discretization of the SFB.

Application to a frictionless channel with a topographic step

Due to the non-conservative form of the bed slope source term, the equation of momentum conservation cannot be solved analytically in the presence of a topographic step. For the purpose of the present theoretical analysis, we focus here on the smallest possible numerical grid which enables a suitable resolution of the problem accounting properly for the typical boundary conditions. Hence, the domain is discretized with two cells on either sides of the topographic step, numbered from 1 (upstream) to 4 (downstream) (Fig. 1).
Substituting Eq. (10) into the discretized formulation of Eq. (4) leads to:

$$\frac{q^2}{\Delta x}\left(\frac{1}{h_i} - \frac{1}{h_{i-1}}\right) + \frac{g}{2}\frac{h_{i+1}^2 - h_i^2}{\Delta x} = -g\frac{2(1-\alpha)h_i + (1-2\alpha)z_{b,i} + 2\alpha h_{i+1} + (2\alpha - 1)z_{b,i+1}}{2}\frac{z_{b,i+1} - z_{b,i}}{\Delta x}. \quad (13)$$

Since the location where a boundary condition is prescribed on the water depth depends on the flow regime, Eq. (13) is solved differently depending on the flow regime.

In the case of a subcritical flow, the water depth h_D is prescribed as a boundary condition on the most downstream cell edge.

Applying Eq. (13) for the four cells described in Fig. 1 leads to:

$$h_U = h_1 = h_2 = h_3 + \Delta z_b \tag{14}$$

$$q^2\left(\frac{1}{h_3}-\frac{1}{h_2}\right)+\frac{g}{2}\left(h_4^2-h_3^2\right)=0 \tag{15}$$

$$\frac{g}{2}h_4^2 = \frac{g}{2}h_D^2 + q^2\left(\frac{1}{h_D}-\frac{1}{h_3}\right). \tag{16}$$

Whatever the value of α, the free surface is found horizontal on either sides of the topographic step.

Grouping the results of Eqs. (14), (15) and (16), the following relationship is obtained between h_U and h_D, independently of the value of α:

$$q^2\left(\frac{1}{h_D}-\frac{1}{h_U}\right)+\frac{g}{2}\left(h_D^2-h_U^2\right)=-g\,\frac{2h_U-\Delta z_b}{2}\Delta z_b. \tag{17}$$

For a supercritical flow, the water depth h_U is set as boundary condition at the most upstream cell edge.

Applying Eq. (13) for the four cells described in Fig. 1 leads to:

$$q^2\left(\frac{1}{h_1}-\frac{1}{h_U}\right)+\frac{g}{2}\left(h_2^2-h_U^2\right)=0 \tag{18}$$

$$q^2\left(\frac{1}{h_D}-\frac{1}{h_1}\right)=-g\left(h_D-\frac{1-2\alpha}{2}\Delta z_b\right)\Delta z_b \tag{19}$$

$$h_2 = h_3 = h_4 = h_D. \tag{20}$$

Grouping the results of Eqs. (18), (19) and (20) leads to:

$$q^2\left(\frac{1}{h_D}-\frac{1}{h_U}\right)+\frac{g}{2}\left(h_D^2-h_U^2\right)=-gh_D\Delta z_b+\frac{1-2\alpha}{2}g\Delta z_b^2. \tag{21}$$

The second term of the bed slope term of Eq. (21) vanishes in the standard discretization of the SFB (α = 1/2).

Non-dimensional forms

To enable systematic numerical evaluations of the energy variations obtained for different Froude numbers and different heights of the topographic step, Eqs. (17) and (21) are rewritten using the non-dimensional parameters defined in Eq. (8):

$$\begin{aligned} &\mathsf{h}^3-\left(1+2\mathsf{F}_U^2\right)\mathsf{h}+\left(2-\Delta\mathsf{z}_b\right)\Delta\mathsf{z}_b\mathsf{h}+2\mathsf{F}_U^2=0 \quad \mathsf{F}_U\le 1\\ &\mathsf{h}^3+2\Delta\mathsf{z}_b\mathsf{h}^2-\left(1+2\mathsf{F}_U^2\right)\mathsf{h}-\left(1-2\alpha\right)\Delta\mathsf{z}_b^2\mathsf{h}+2\mathsf{F}_U^2=0 \quad \mathsf{F}_U\ge 1. \end{aligned} \tag{22}$$

Energy variation

Similarly, the non-dimensional energy variation between upstream and downstream

writes as:

$$\Delta E = \frac{E_U - E_D}{E_U} = \frac{F_U^2 + 2 - \frac{1}{h^2}F_U^2 - 2h - 2\Delta z_b}{F_U^2 + 2}. \quad (23)$$

For a given value of α and a given upstream Froude number F_U, the energy variation resulting from the resolution of the discretized momentum equation may be quantified using the following indicators, namely the bias and the root-mean-square (RMS):

$$\text{bias}(F_U, \alpha) = \langle \Delta E \rangle \quad (24)$$

$$\text{RMS}(F_U, \alpha) = \sqrt{\langle \Delta E^2 \rangle}. \quad (25)$$

Where the operator $\langle ... \rangle$ refers to an average over all non-dimensional step heights Δz_b between $\Delta z_b = -1$ and $\Delta z_b = 1$. The discretization step for Δz_b was selected small enough so that the values of bias and RMS are independent of this discretization.

The bias represents the arithmetic mean of the numerical energy variation among all the considered topographic steps. A positive value reflects dominant energy dissipation while a negative value represents dominant energy creation. The RMS represents the energy variation in absolute term for a given value of α and a given Froude number.

2.2 Results and discussion

Comparison between the exact solutions of the equation of conservation of mechanical energy and the solutions of the discrete equation of momentum conservation

The solutions of the non-dimensional Eq. (22) are shown in Fig. 2 for the standard discretization of the SFB (α = 1/2 in dashed lines) and for the standard discretization of the DFB (α = 0 in dotted lines). The discrete solutions of the equation of momentum conservation are compared to the exact solution of the equation of energy conservation (plain lines). For negative (respectively positive) topographic steps, the zones representing subcritical or supercritical flows are, respectively, labelled zones 1 and 2 (respectively zones 4 and 3).

For negative topographic steps $(\Delta z_b < 0)$ in Fig. 2a, the two curves in black represent the limits corresponding to an upstream Froude number tending towards unity, either from subcritical (upper curve) or from supercritical (lower curve) flow regimes. These limits cannot be reached for positive topographic steps (Fig. 2b) since critical flow corresponds to the minimum energy for a given discharge and, therefore, an approaching critical flow could not adapt to a positive topographic step.

For positive topographic steps $(\Delta z_b > 0)$ in Fig. 2b, the limits for a downstream Froude tending towards unity from subcritical (lower curve) and supercritical (upper curve) flows are the curves in grey.

The discontinuous black line in Fig. 2 represents the hypothetical limit of an infinite Froude number, in which case the water depth remains unaffected by the topographic step due to the high kinetic energy.

Figure 2 presents in dashed line the solutions of the discrete form of the momentum conservation equation with the standard discretization of the SFB (or the discretization of the DFB with the particular value of α = 1/2). Although these results are similar to those of the analytical energy conservation, they are not exactly the same. The main differences appear for a positive topographic step in supercritical flow (e.g., $F_U = 2$ in zone 3), for which two different flow conditions may be obtained for the same value of Δz_b and without change of the flow regime.

Figure 2 presents in dotted line the solution of the discrete form of the momentum conservation equation with the standard discretization of the DFB (α = 0). For subcritical flow, the solutions of the discrete momentum conservation equations with the standard discretization of the SFB and with the standard discretization of the DFB are identical, consistently with the independency of the corresponding part of Eq. (22) with respect to α. In contrast, for supercritical flows, the solutions are similar but not equal. The difference between the solution obtained with the energy conservation and the solution obtained with the momentum conservation with the standard discretization of the DFB tends to increase with the absolute value of the topographic step. While the momentum conservation with the standard discretization of the SFB only gives overestimations of the parameter h in supercritical flows, the momentum conservation with the standard discretization of the DFB overestimates or underestimates the values of h depending on the value of Δz_b.

Energy variation of the discrete resolution of the momentum conservation equations

As shown in plain lines in Fig. 3, only positive energy losses are observed with the standard discretization of the SFB, indicating that the discretization of the momentum conservation induces only numerical *dissipation* of energy. This dissipation tends to increase with the absolute height of the topographic. The range of variation of energy losses for subcritical and supercritical flows are represented in light grey with respectively circular markers and arrows at the tips. Moreover, for a given height of the topographic step, the dissipation is maximum for Froude numbers close to unity. For positive topographic steps (Fig. 3a), the dissipation obtained in supercritical flow conditions generally exceeds the dissipation for subcritical flow.

The energy variation resulting from the discrete resolution of the momentum conservation equation with the standard discretization of the DFB is represented in dotted lines in Fig. 3. Negative energy losses are obtained for supercritical flows with a negative topographic step (Fig. 3a) and for some supercritical flows with a positive topographic step (Fig. 3b). For negative topographic steps, the magnitude of the numerical energy variation increases when the Froude number becomes closer to unity, while it is not necessary the case for positive topographic steps (e.g., $F_U = 2.0$).

Energy variations for subcritical flows are identical for both formulations of the bed slope term. Concerning supercritical flows with the standard discretization of the DFB ($\alpha = 0$), numerical energy is created for negative topographic steps with absolute values greater than the dissipation of energy with the standard discretization of the SFB.

Optimal values of α to minimize the numerical energy variation

As shown in Fig. 4a, for supercritical flows, the bias of energy is negative (i.e. dominating energy creation) for lowest values of α and positive (i.e. dominating energy dissipation) for highest ones. Whatever the value of α, the RMS tends towards zero for high upstream Froude numbers and is the highest for upstream Froude numbers close to one (Fig. 4b).

Figure 5 shows the optimal values of α, i.e. those values which minimize the energy variation resulting from the numerical discretization. The values minimizing the bias are found slightly lower than those minimizing the RMS for upstream Froude numbers up to slightly more than 2. For higher upstream Froude numbers, the values of α minimizing the bias are very close to those which minimize the RMS. In any case, the variation of the optimal value of α with the upstream Froude number is found particularly low. In practice, this suggests the use of a single value of α ($\alpha = 0.4$) whatever the upstream Froude number. This rule of thumb guarantees that the numerical energy variation remains always very close to its minimum. This optimal value of α is based on the minimization of the error on the energy whatever the remaining error should be a reduction or an augmentation of mechanical energy. When searching for a minimization of the numerical energy without any creation of energy, the optimal value of α is close to 0.5 which leads however to an increase of the RMS compared to a value of $\alpha = 0.4$.

3 Numerical analysis

The sensitivity of the numerical variation of mechanical energy to the discretization of the DFB is numerically analyzed for a 1D steady flow over a slopeless and frictionless

channel with a bump [2] and for a 1D dam break flow over a channel with a bump, with and without friction. The first test case is a standard test case, often used to evaluate the accuracy of the treatment of the bed slope term by numerical models, as well as their efficiency to converge towards a steady solution [15,16,32]. The second test case is consider to assess the validity of our conclusions in cases with unsteadiness and friction.

Four discretizations of the DFB are tested: $\alpha = 0.0$ which is equivalent to the standard discretization of the DFB, $\alpha = 0.4$ hereabove presented as an optimal discretization, $\alpha = 0.5$ referred to as the standard SFB discretization and $\alpha = 1.0$.

3.1 1D steady flow over a slopeless and frictionless channel

Methods

The bottom level is given by Eq. (26) $(-10\,m \le x \le 10\,m)$:

$$z(x) = \begin{cases} 0.8\left(1 - \dfrac{x^2}{4}\right) & -2\,m \le x \le 2\,m \\ 0 & \text{elsewhere} \end{cases}. \tag{26}$$

Two different sets of boundary conditions are analyzed (Table 1). The first one leads to a subcritical flow while the second one corresponds to a supercritical flow. There is no hydraulic jump and, in the exact solution, the energy is therefore constant over the entire domain (assuming no friction within the fluid). For each test case, range of Froude number and energy value are given in Table 1.

The two tests are simulated with the hydraulic model Wolf2D, in which the DFB has been implemented. The model solves the fully dynamic shallow-water equations using a conservative finite volume scheme based on a flux vector splitting technique [9,11]. The computational domain is discretized with a 0.1 m grid spacing.

The mechanical energy at a border is evaluated by Eq. (27), consistently with the flux-vector splitting technique:

$$E_{i+1/2} = \eta_{i+1} + \frac{1}{2g}\frac{q_{x,i}^2}{h_{x,i}^2}. \tag{27}$$

The differences between the analytical solution and the numerical ones are quantified with the L_1 error defined by Eq. (28):

$$L_1(y) = \frac{1}{N}\sum_{i=1}^{N}\left|\frac{y_{i,num} - y_{i,ref}}{y_{i,ref}}\right| \tag{28}$$

where N is the number of computational cells, $y_{i,num}$ is a numerical solution and $y_{i,ref}$ is the analytical solution.

Results and discussion

The water depths are more sensitive to the discretization of the bed slope term for supercritical flows than for subcritical ones (Fig. 6 and Table 2). For a supercritical flow, the order of magnitude of the differences between the water depths resulting from different discretizations of the bed slope term highlights the necessity of an accurate discretization of the bed slope term.

As shown in Fig. 7, the numerical variations of energy are produced at the bump and propagate towards upstream for a subcritical flow (Fig. 7a) and towards downstream for a supercritical flow (Fig. 7b). In the first test, the errors on the energy increase when the value of α decreases, while, for the second test case, the errors increase when the value of α moves away from the value of $\alpha = 0.4$. Concerning the second test case with a supercritical flow, dissipation of energy occurs for values of α equal to 0.5 and 1.0 while creation of energy occurs for $\alpha = 0.0$, consistently with the results presented in Fig. 4.

As shown in Table 2, the error on energy may change by two orders of magnitude depending on the discretization of the DFB for supercritical flows while they show a lower sensitivity to the value of α for subcritical flows. Moreover, the order of magnitude of the lowest energy error for the second test is the same as the one obtained for the first test case, whatever the value of α. These results are consistent with the selection of an optimal value of α=0.4 for the discretization of the DFB, as concluded from the theoretical analysis in section 2.

3.2 1D dam break flow over a channel with a bump

Methods

This test case is based on an experimental setup [1] realized at the Laboratory of Hydraulic Research of Chatelet (Belgium). It consists in a dam break flow over a rectangular channel with a bump (Fig. 8). Both the upstream (A) and downstream (B) ends are impervious plates. The channel is 38 m long (L_R) and a 15.5 m long and 0.75 m deep (h_0) water volume is initially retained at the upstream end by a sluice gate. The top of a symmetrical 6 m long and 0.4 m high bump is located 13 m downstream of the gate. The simulations were performed for (i) a frictionless channel and (ii) a channel with a uniform Manning coefficient $n = 0.0125$ s/m$^{1/3}$.

Since the flow is unsteady, the inertia effects must be taken into account to assess the energy conservation in the computed results. To do this, we consider hereafter the sum of *(i)* the energy head integrated over the whole flow area and *(ii)* the corresponding inertia term.

The energy head E at any position (x,z) of the flow is the sum of the potential energy z, the pressure energy η-z and the kinetic energy $u^2/2g$ at that point. Since the pressure is hydrostatic and the velocity uniform, the energy head is constant over the depth:

$$E(x,t) = \eta(x,t) + \frac{u(x,t)^2}{2g}. \tag{29}$$

The unsteady Bernouilli equation between two points x_i and x_j writes:

$$E(x_i,t) = E(x_j,t) + \int_{x_i}^{x_j} \frac{1}{g}\frac{\partial u}{\partial t} dx \tag{30}$$

where the second term of the right hand side represents the inertia contribution (E_I).

At a time t, the total mechanical energy Σ is defined as the sum of the integration over the whole flow area of the energy head E and of the inertia contribution E_I:

$$\Sigma(t) = \int_A^B \left[h(x,t)\left(\eta(x,t) + \frac{u(x,t)^2}{2g} \right) + h(x,t)\int_A^x \frac{1}{g}\frac{\partial u(x',t)}{\partial t} dx' \right] dx, \tag{31}$$

where A and B are the abscissa of the channel upstream and downstream boundaries.

For an unsteady inviscid flow over a frictionless channel, Σ is constant over time and remains equal to its initial value $L_R h_0^2$ (= 8.7187 m^3) provided that the flow does not reach the boundaries of the domain.

Results and discussion

For gauges G4 and G13 (Fig. 8), the time evolutions of the water depth are represented in Fig. 9 for different values of α and for a channel with or without friction. At both gauges, the maximum water depth of the dam break wave depends significantly on the value of α, particularly at G4 with a frictionless channel where the maximum water depth reached by the wave for α = 0.0 is 8 cm above the value obtained for α = 0.5. The highest differences between the water depths obtained with a value of α = 0.4 and with the other values of α are of the order of 10^{-1} m at G4 and of 10^{-2} m at G13. Time logs are also observed between the time evolutions of computed water depths from different values of α, particularly at gauge G4. This suggests that the discretization of the bed slope term may have a significant impact on the results of a simulation of a dam break flow, both in terms of computed water depths and propagation times.

In Fig. 10, the time evolutions of Σ for different values of α are compared to those obtained for the reference value α = 0.4, for a channel with (b) or without (a) friction. The time period represented in Fig. 10 is such that the boundaries of the domain are not reached. The deviations of Σ as a function of α remain relatively small compared to the initial value of

$\Sigma = L_R h_0^2$ (with a maximum relative difference of the order of 0.1%); but they increase very fast with time. The results are consistent with those obtained from the theoretical analysis and from the 1D steady flow with the bump (Fig. 7b); i.e. an increase (resp. decrease) of the numerical variation of energy when the value of α is reduced (resp. increased) for a supercritical flow. The results obtained for a channel with friction are similar to the case of the frictionless channel, with mainly a time shift due to a reduction of the front velocity in the presence of friction.

4 Conclusions

Solving the discrete equation of momentum conservation induces numerical variations of energy, even in the case of a flow in a frictionless channel without physical energy dissipation.

In this paper, we compare the resolution of the discrete equation of momentum conservation for two formulations of the bed slope term. The standard formulation of the bed slope term (SFB) involves the product of the water depth by the spatial derivative of the topographic level. The divergence formulation of the bed slope term (DFB) consists in evaluating the bed slope term as the spatial variation of the pressure assuming a constant free surface elevation.

A major difference in the results obtained with the two formulations of the bed slope term is that the discretization of the SFB induces only positive energy losses (i.e. dissipation of energy) while positive and negative energy losses are obtained with the discretization of the DFB.

An optimal discretization of the DFB, i.e. a scheme minimizing the numerical variation of energy, is proposed based on the theoretical analysis of the numerical variation of energy for a 1D continuous, slopeless and frictionless flow with a topographic step. Finally, two numerical test cases show results in good agreement with the findings of the theoretical analysis and highlight the practical relevance to minimize the energy variation due to the discretization of the bed slope term.

Acknowledgements

The research was funded through the ARC grant for Concerted Research Actions, financed by the Wallonia-Brussels Federation.

Notation

A = the abscissa of the channel upstream boundary (m)

B = the abscissa of the channel downstream boundary (m)

E = energy head (m)

E_I = inertial contribution to the unsteady mechanical energy (m)

F = Froude number (-)

h = water depth (m)

h = non-dimensional water depth (-)

g = gravity acceleration (ms^{-2})

q = unit discharge (m^2s^{-1})

x = spatial coordinate (m)

t = time (s)

z_b = bottom elevation (m)

α = parameter controlling the discretization of the divergence formulation of the bed slope term (-)

$\Delta\mathsf{E}$ = non-dimensional energy variation (-)

$\Delta\mathsf{z}_b$ = non-dimensional topographic step (-)

η = free surface level (m)

Σ = total mechanical energy (m^3)

References

[1] F. Alcrudo, S. Soares-Frazão, Conclusions from the 1st CADAM meeting - Wallingford UK. Concerted Action on Dam-Break Modeling – Proc. CADAM meeting Wallingford, United Kingdom 2 and 3 March 1998, European Commission, Brussels, 35–43, 1999.

[2] F. Aureli, A. Maranzoni, P. Mignosa, C. Ziveri, A weighted surface-depth gradient method for the numerical integration of the 2D shallow water equations with topography, Advances in Water Resources 31 (2008) 962-974.

[3] A. Bermúdez, A. Dervieux, J. A. Desideri, M. E. Vázquez, Upwind schemes for the two-dimensional shallow water equations with variable depth using unstructured meshes, Computer Methods in Applied Mechanics and Engineering 155 (1-2) (1998) 49-72.

[4] A. Bermúdez, M. E. Vázquez, Upwind methods for hyperbolic conservation laws with source terms, Computers and Fluids 23 (8) (1994) 1049-1071.

[5] M. Bruwier, P. Archambeau, S. Erpicum, M. Pirotton, B. Dewals, Assessing the operation rules of a reservoir system based on a detailed modelling-chain, Natural Hazards and Earth System Sciences 15(3) (2015) 365-379.

[6] O. Castro-Orgaz, J. V. Giráldez, J. L. Ayuso, Energy and momentum under critical flow conditions, Journal of Hydraulic Research 46:6 (2008) 844-848.

[7] P. Costabile, C. Costanzo, F. Macchione, Comparative analysis of overland flow models using finite volume schemes, Journal of Hydroinformatics 14 (1) (2012) 122-135.

[8] P. Costabile, F. Macchione, Enhancing river model set-up for 2-D dynamic flood modelling, Environmental Modelling and Software 67 (2015) 89-107.

[9] B. J. Dewals, S. A. Kantoush, S. Erpicum, M. Pirotton, A. J. Schleiss, Experimental and numerical analysis of flow instabilities in rectangular shallow basins, Environmental Fluid Mechanics 8 (1) (2008) 31-54.

[10] S. Erpicum, Optimisation objective de paramètres en écoulements turbulents à surface libre sur maillage multibloc, Phd Thesis, University of Liege (ULG), Belgium, 2006 [in french].

[11] S. Erpicum, B. J. Dewals, P. Archambeau, M. Pirotton, Dam-break flow computation based on an efficient flux-vector splitting, Journal of Computational and Applied Mathematics 234 (2010a) 2143-2151.

[12] S. Erpicum, B. J. Dewals, P. Archambeau, S. Detrembleur, M. Pirotton, Detailed inundation modelling using high resolution DEMs, Engineering Applications of Computational Fluid Mechanics 4 (2010b) 196-208.

[13] W. G. Field, M. F. Lambert, B. J. Williams, Energy and momentum in one dimensional open channel flow, Journal of Hydraulic Research 36 (1) (1998) 29-42.

[14] P. Garcia-Navarro, M. E. Vázquez, On numerical treatment of the source terms in the shallow water equations, Computers and Fluids 29 (8) (2000) 951-979.

[15] J. Hou, Q. Liang, F. Simons, R. Hinkelmann, A 2D well-balanced shallow flow model for unstructured grids with novel slope source term treatment, Advances in Water Resources 52 (2013a) 107-131.

[16] J. Hou, Q. Liang, F. Simons, M. Mahgoub, R. Hinkelmann, A robust well-balanced model on unstructured grids for shallow water flows with wetting and drying over complex topography, Computer Methods in Applied Mechanics and Engineering 257 (2013b) 126-149.

[17] M. E. Hubbard, Multidimensional Slope Limiters for MUSCL-Type Finite Volume Schemes on Unstructured Grids, Journal of Computational Physics 155 (1) (1999) 54-74.

[18] G. Kesserwani, Topography discretization techniques for Godunov-type shallow water numerical models: A comparative study, Journal of Hydraulic Research 51 (4) (2013) 351-367.

[19] B. Kim, B. F. Sanders, J. E. Schubert, J. S. Famiglietti, Mesh type tradeoffs in 2D hydrodynamic modeling of flooding with a Godunov-based flow solver, Advances in Water Resources 68 (2014) 42-61.

[20] R. J. LeVeque, Balancing Source Terms and Flux Gradients in High-Resolution Godunov Methods: The Quasi-Steady Wave-Propagation Algorithm, Journal of Computational Physics 146 (1) (1998) 346-365.

[21] Q. Liang, F. Marche, Numerical resolution of well-balanced shallow water equations with complex source terms, Advances in Water Resources 32 (6) (2009) 873-884.

[22] J. Murillo, P. Garcia-Navarro, Energy balance numerical schemes for shallow water equations with discontinuous topography, Journal of Computational Physics 236 (1) (2013) 119-142.

[23] J. Murillo, P. Garcia-Navarro, Accurate numerical modeling of 1D flow in channels with arbitrary shape. Application of the energy balanced property, Journal of Computational Physics 260 (1) (2014) 222-248.

[24] M. Nujic, Efficient implementation of non-oscillatory schemes for the computation of free-surface flows, Journal of Hydraulic Research 33 (1) (1995) 101-111.

[25] B. F. Sanders, J. E. Schubert, H. A. Gallegos, Integral formulation of shallow-water equations with anisotropic porosity for urban flood modeling, Journal of Hydrology 362 (1-2) (2008) 19-38.

[26] J. E. Schubert, B. F. Sanders, Building treatments for urban flood inundation models and implications for predictive skill and modeling efficiency, Advances in Water Resources 41 (0) (2012) 49-64.

[27] J. Singh, M. S. Altinakar, Y. Ding, Two-dimensional numerical modeling of dam-break flows over natural terrain using a central explicit scheme, Advances in Water Resources 34 (10) (2011) 1366-1375.

[28] G. S. Stelling, S. P. A. Duinmeijer, A staggered conservative scheme for every Froude number in rapidly varied shallow water flows, International Journal for Numerical Methods in Fluids 43 (12) (2003) 1329-1354.

[29] F. Stilmant, M. Pirotton, P. Archambeau, S. Erpicum, B. Dewals, Can the collapse of a fly ash heap develop into an air-fluidized flow? - Reanalysis of the Jupille accident (1961), Geomorphology 228 (2015) 746-755.

[30] P. K. Tonnon, L. C. van Rijn, D. J. R. Walstra, The morphodynamic modelling of tidal sand waves on the shoreface, Coastal Engineering 54 (4) (2007) 279-296.

[31] A. Valiani, V. Caleffi, A. Zanni, Case study: Malpasset dam-break simulation using a 2D finite-volume method, Journal of Hydraulic Engineering 128 (5) (2002) 460-472.

[32] A. Valiani, L. Begnudelli, Divergence form for bed slope source term in shallow water equations, Journal of Hydraulic Engineering 132 (7) (2006a) 652-665.

[33] A. Valiani, L. Begnudelli, Discussion of ‘‘Divergence form for bed slope source term in shallow water equations” by Alessandro Valiani and Lorenzo Begnudelli, Journal of Hydraulic Engineering 134 (5) (2006b) 680–682.

[34] M. E. Vázquez, Improved Treatment of Source Terms in Upwind Schemes for the Shallow Water Equations in Channels with Irregular Geometry, Journal of Computational Physics 148 (2) (1999) 497-526.

[35] W. Wu, S. Y. Wang, One-dimensional modeling of dam-break flow over movable beds, Journal of Hydraulic Engineering 133 (1) (2007) 48-58.

[36] J. G. Zhou, D. M. Causon, C. G. Mingham, D. M. Ingram, The Surface Gradient Method for the Treatment of Source Terms in the Shallow-Water Equations, Journal of Computational Physics 168 (1) (2001) 1-25.

Table 1: Boundary conditions, analytical Froude range and analytical energy for a 1-D steady flow over a bump.

Test ID	Upstream boundary condition	Downstream boundary condition	Analytical F range	Analytical energy
1	$q = 1 m^2/s$	$h_D = 1.7 m$	0.14 - 0.41	$E_{exact} = 1.718 m$
2	$q = 1.5 m^2/s; h_U = 0.25 m$	Transmissive	2.31 - 3.83	$E_{exact} = 2.085 m$

Table 2: Errors on the water depths, unit discharges and mechanical energy for four discretizations of the DFB.

Test ID	α	$L_1(h)$	$L_1(E)$
1	0.0	3.2×10^{-3}	2.8×10^{-3}
	0.4	2.5×10^{-3}	2.1×10^{-3}
	0.5	2.4×10^{-3}	1.9×10^{-3}
	1.0	1.5×10^{-3}	1.1×10^{-3}
2	0.0	5.9×10^{-3}	66.3×10^{-3}
	0.4	1.2×10^{-3}	1.6×10^{-3}
	0.5	2.2×10^{-3}	18.3×10^{-3}
	1.0	10.1×10^{-3}	100.7×10^{-3}

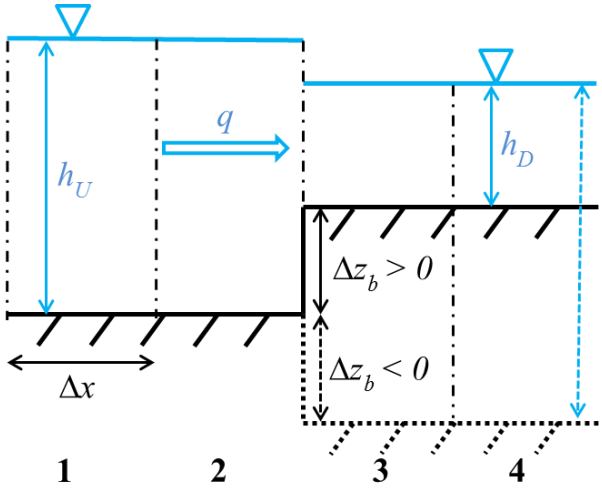

Figure 1: 1D channel with a topographic step.

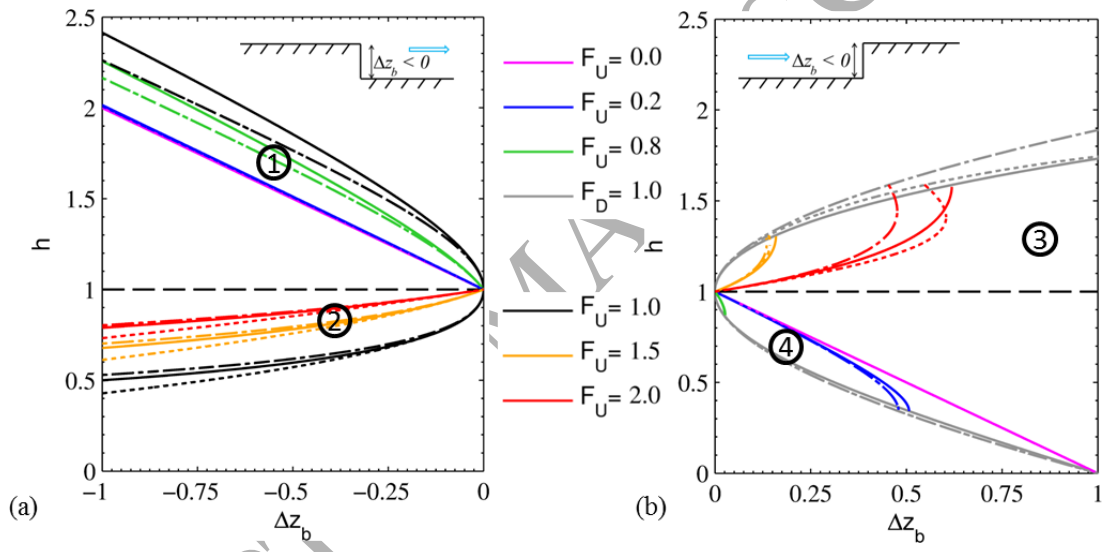

Figure 2: Hydrodynamic characteristics $(h, \Delta z_b)$ for a flow in a slopeless and frictionless 1D channel with a (a) negative or (b) positive topographic step – Comparison between the exact resolution of energy conservation (plain lines), the momentum conservation discretized with the standard discretization of the SFB (dashed lines) and the momentum conservation discretized with the standard discretization of the DFB (dotted lines). For negative (respectively positive) topographic steps, the zones representing subcritical or supercritical flows are respectively labelled zones 1 and 2 (respectively zones 4 and 3).

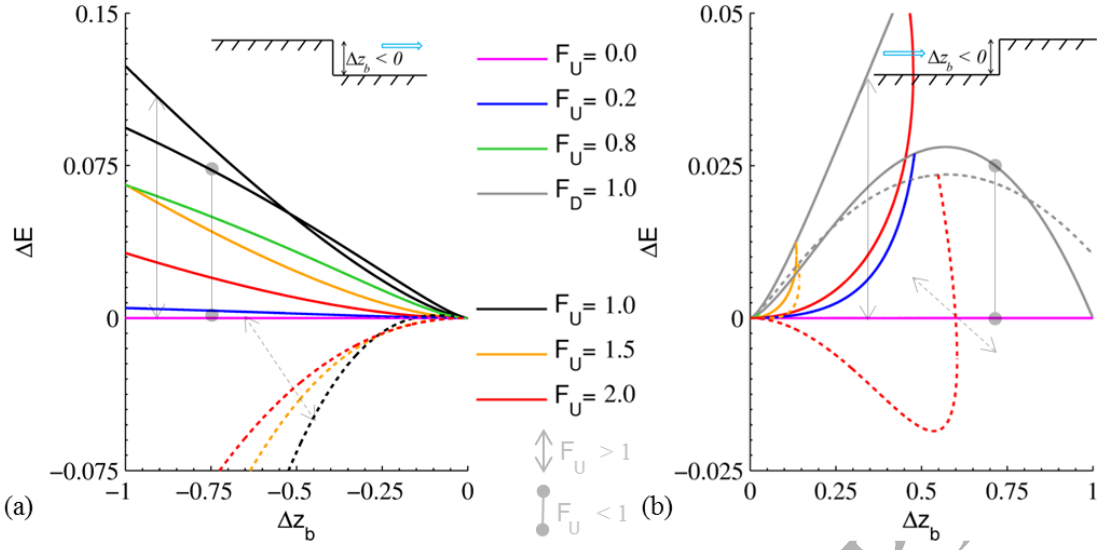

Figure 3: Energy loss accross a topographic step in a slopeless and frictionless 1D channel - Comparison between the momentum conservation with the standard discretization of the SFB (plain lines) and the momentum conservation with the standard discretization of the DFB (α = 0) (dotted lines).

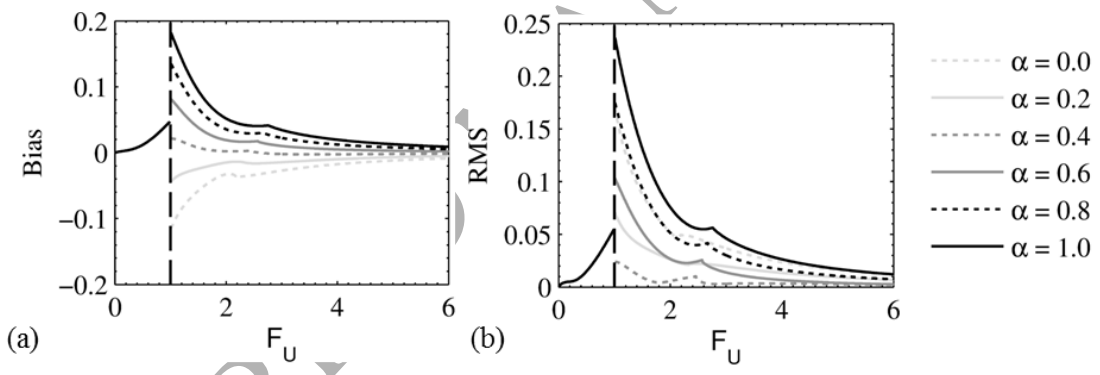

Figure 4: Bias and RMS of the numerical variation of energy as a function of the upstream Froude number for different values of α in the discrete momentum conservation equation with the DFB.

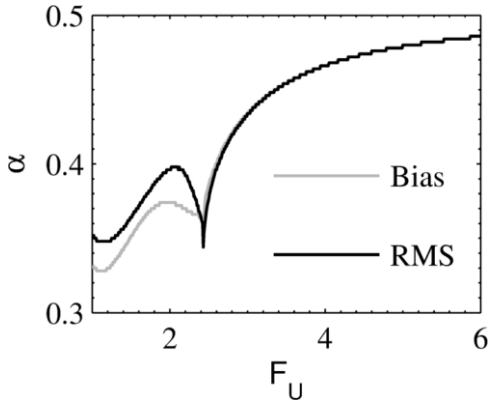

Figure 5: Value of α minimizing the bias or the RMS of the numerical variation of energy for different upstream Froude numbers.

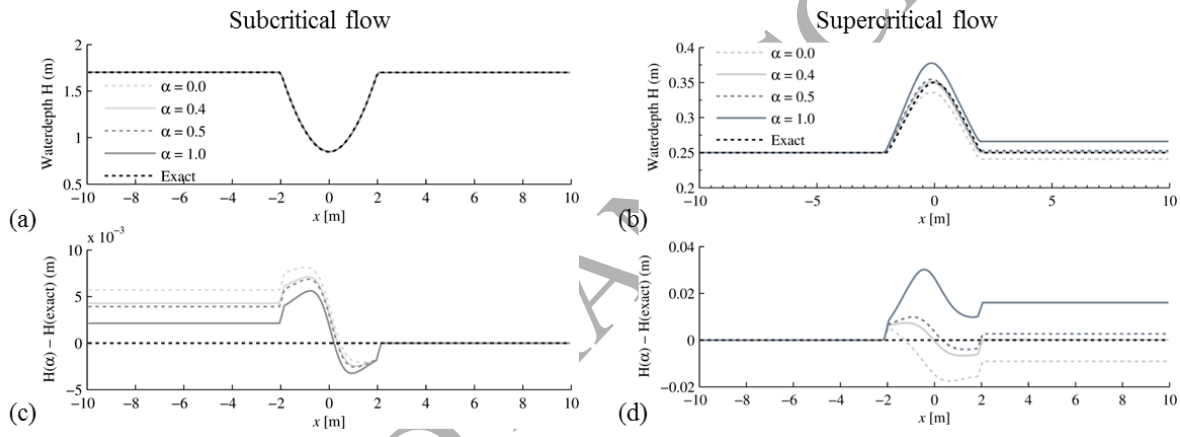

Figure 6: Water depths (a, b) and energy variation (c, d) for a 1D steady flow over a bump and different values of α.

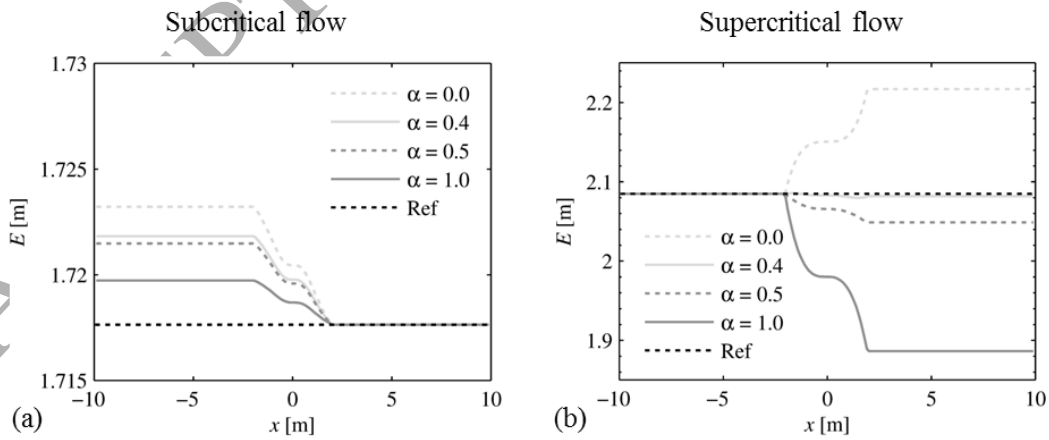

Figure 7: Comparison of the mechanical energy between the analytical solution (black line) and the computed results for a 1D steady flow over a bump and different values of α.

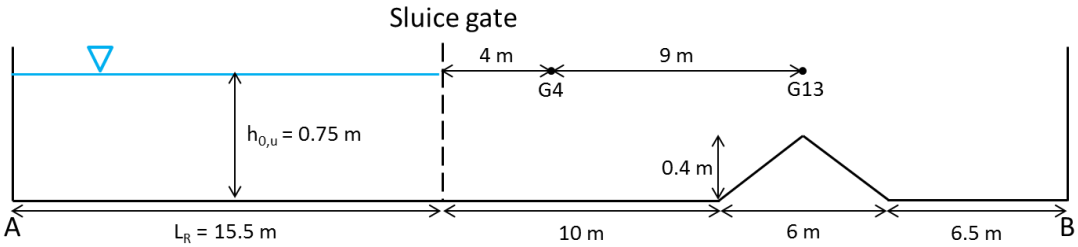

Figure 8: Schematization of the test case of a 1D dam break flow over a channel with a bump.

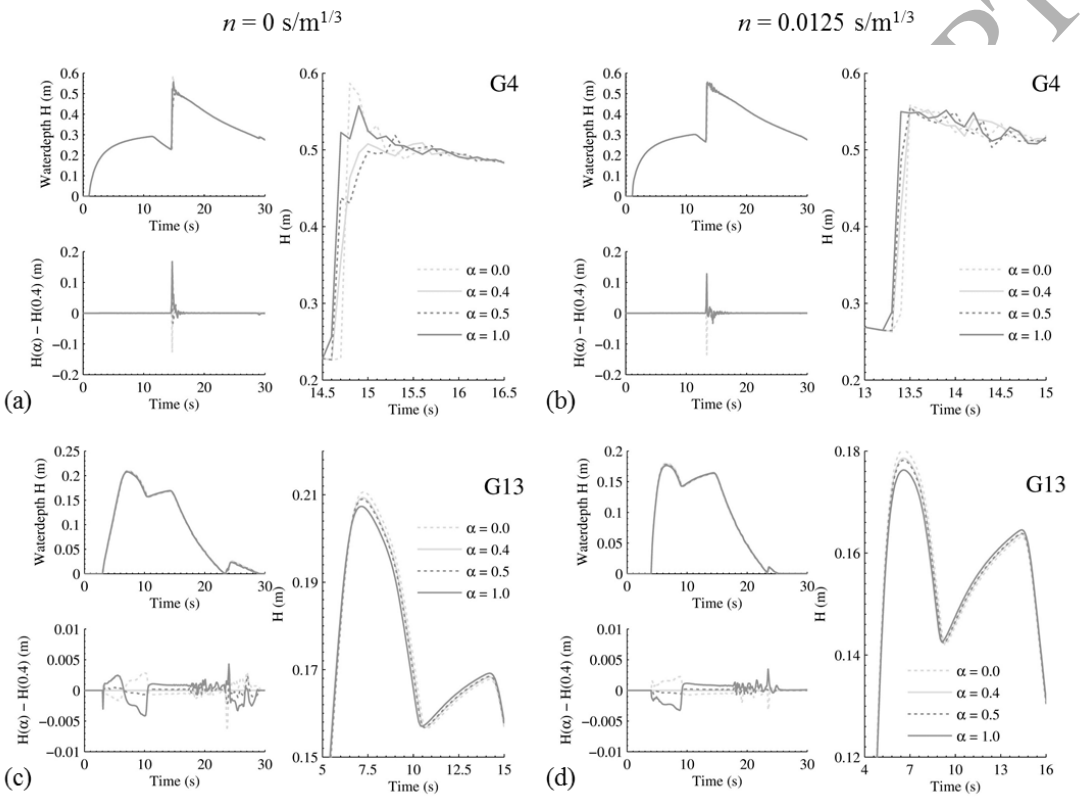

Figure 9: Time evolution of the water depth at gauges G4 (a, b) and G20 (c, d) for different discretizations of the bed slope term and for a channel with (b, d) or without (a, c) friction.

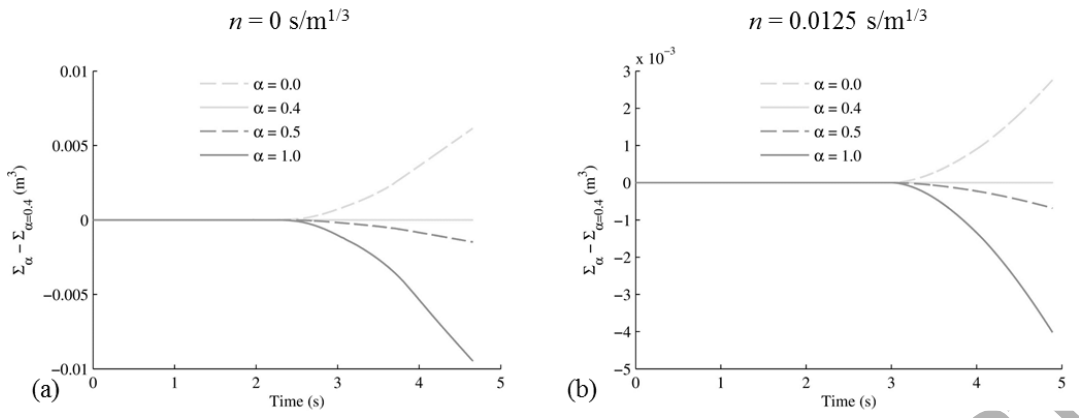

Figure 10: Comparison of the time evolution of the total energy Σ for $\alpha = 0.4$ to other discretizations of the bed slope term for a channel with (a) or without (b) friction.